

# Measurement of the ortho-positronium confinement energy in mesoporous thin films

Paolo Crivelli\*

*Instituto de Física, Universidade Federal do Rio de Janeiro (UFRJ),  
Rio de Janeiro, 21941-972, Brazil*

Ulisse Gendotti<sup>†</sup> and André Rubbia

*Institut für Teilchenphysik, ETHZ,  
CH-8093 Zürich, Switzerland*

Laszlo Liskay<sup>‡</sup> and Patrice Perez

*CEA, Saclay, IRFU, 91191 Gif-sur-Yvette Cedex, France*

Catherine Corbel

*LSI, Ecole polytechnique, Route de Saclay,  
91128, Palaiseau cedex, France*

(Dated: February 8, 2010)

In this paper, we present measurements of the ortho-positronium emission energy in vacuum from mesoporous films using the time of flight technique. We show evidence of quantum mechanical confinement in the mesopores that defines the minimal energy of the emitted Ps. Two samples with different effective pore sizes, measured with positron annihilation lifetime spectroscopy, are compared for the data collected in the temperature range 50-400 K. The sample with smaller pore size exhibits a higher minimal energy ( $\simeq 73$  meV), compared to the sample with bigger pores ( $\simeq 48$  meV), due to the stronger confinement. The dependence of the emission energy with the temperature of the target is modeled as ortho-positronium being confined in rectangular boxes in thermodynamic equilibrium with the sample. We also measured that the yield of positronium emitted in vacuum is not affected by the temperature of the target.

PACS numbers: Valid PACS appear here

## I. INTRODUCTION

The Positronium (Ps), the bound state of electron and positron, was extensively investigated since its discovery [1] contributing to the development of bound state QED [2]. Furthermore, this system provided stringent limits on possible deviation from the Standard Model that could indicate new physics [3, 4]. Moreover, in the field of materials science Ps found various applications due to its unique properties (see e.g. [5, 6] for modern reviews on this subject). One recent example is the characterization via positron annihilation lifetime spectroscopy (PALS) of low-k dielectrics that are potential candidates for the next generation of integrated circuits [7, 8]. The motivation of the work presented in this paper is to understand if this kind of mesoporous silica with interconnected pore network could be used for producing a high fraction of positronium at low temperatures. This would open the

door for a new generation of experiments in fundamental research. Cold positronium could be used to improve the precision of spectroscopic studies of Ps, perform the first spectroscopy of the Ps<sub>2</sub> molecule [9], be used for anti-hydrogen formation via charge-exchange for anti-gravity test [10, 11] or to confirm the interpretation of the recent DAMA/LIBRA annual modulation signal [12, 13] as generated by Mirror type dark matter [14]. A step further would be to initiate a novel physics by achieving Bose-Einstein condensation of Ps [15].

In mesoporous silica, Ps is produced by injecting positrons into the film and the distribution of the implantation depth follows a Makhovian profile [16]. In the following we solely consider the long lived triplet spin state (called ortho-positronium with 142 ns lifetime, o-Ps) because the singlet spin state (called para-positronium, p-Ps) has a very short lifetime of 125 ps and can be considered as annihilating in the target. The o-Ps (for simplicity we will refer to it as Ps) that diffuses into the pores loses its kinetic energy via scattering. If the pores are interconnected, Ps has a probability to tunnel from one pore to the other. A fraction of Ps reaches the film surface and exits into vacuum where its energy has a minimum. A classical model of thermalization process was developed by Nagashima et al. [17]. Their calculations

---

\*Electronic address: paolo.crivelli@cern.ch

<sup>†</sup>Electronic address: ulisse.gendotti@cern.ch

<sup>‡</sup>On leave from KFKI Research Institute for Nuclear and Particle Physics, P.O. Box 49, H-1525 Budapest, Hungary

reproduce very well the behavior for the SiO<sub>2</sub> aerogel with pore sizes of about 100 nm. However, a classical approach is not expected to give reliable predictions for Ps confined in few nm pores because quantum mechanical effects become relevant. As a matter of fact, in this regime the de Broglie thermal wavelength of Ps is comparable with the size of the pores. Recently, Mariazzi et al [18] considered phonon scattering to reproduce the thermalization process of Ps in a box (closed porosity) showing that the minimal energy is not the one of the lowest accessible level because the momentum phonons can exchange is fixed. In the same paper, they pointed out that this is not the case in rectangular channels because in one direction the side of the potential well tends to infinity (z-axis). Therefore, the magnitudes of the  $k_x$  and  $k_y$  momentum are quantized but the  $k_z$  tends to be a continuum and the minimal energy that Ps can reach is given by the ground state in the x-y components.

In previous studies of Ps emission in vacuum using time of flight (TOF), many interesting effects, such as the emission from the surface of different materials [19]-[21] were investigated. Recently, this technique was applied to study mesoporous and hybrid silica films [22]-[27], to evaluate the continuity barrier [28] and the effect of thermalization for pore surfaces decorated with different groups [29]. However, the influence of the temperature on Ps emission in vacuum from mesoporous thin films was never studied in detail. To our knowledge, only a work of Mills et al. [21] with fumed silica revealed a dependence with the temperature of the Ps emission in vacuum. The fraction of Ps in the low energy tail was estimated but no quantitative estimate on the value of the minimal emission energy was obtained.

In this paper, we study two different kinds of mesoporous thin films with the same tetraethoxysilane (TEOS) mineral source for the silica network skeleton precursor: CTACl-TEOS and F127-TEOS. The density of C the sample is approximately 1.2 g/cm<sup>3</sup> and of the F sample is 1.5 g/cm<sup>3</sup>. Both samples were spin-coated on glass similar to the ones we measured in [30]. The CTACl-TEOS (called hereafter C sample) are prepared via sol-gel process using cetyl trimethyl ammonium chloride (CTACl) cationic surfactants as the organic pore generator (porogen) agent [31]. A pure aqueous method is used. The CTACl/TEOS molar ratio for the films prepared is 0.22. After deposition, the CTACl-TEOS/Glass samples are treated at 130 °C and stored in air. The F127-TEOS (called hereafter F sample) use non-ionic Pluronic F-127 triblock copolymer (EO<sub>106</sub>PO<sub>70</sub>EO<sub>106</sub>) as surfactant and were prepared in the same way as described in [32]. Both samples were calcinated for 15 minutes at 450 °C in air immediately before the e<sup>+</sup> measurements. The recorded X-ray diffraction patterns indicate no symmetry in the pore organization.

## II. DESCRIPTION OF THE EXPERIMENTAL APPARATUS

### A. Slow positron beam

The ETHZ slow positron beam used for these measurements is described in greater detail in [33]. The positrons flux is 25000 e<sup>+</sup>/s. The slow positron beam is stopped in the SiO<sub>2</sub> target. The positrons can either form positronium, i.e. o-Ps or p-Ps, or annihilate into 2γ's. The detection with an MCP (Micro-channel Plate) of the secondary electrons emitted when the positrons hit the target serves for tagging the positronium formation. The secondary electrons (SE) leave the target accelerated to 1-11 keV by the same voltage applied to the target relative to the grounded transport tube that is used to implant the positrons in the positronium converter. The secondary electrons are then transported by a magnetic field in the backward direction, as shown in Figure 1. The electrons move along the magnetic field line in spirals and are deflected to the micro-channel plate (MCP) region by the  $E \times B$  filter. The tagging efficiency varies from 70% to 30% in the energy range 1-10 keV.

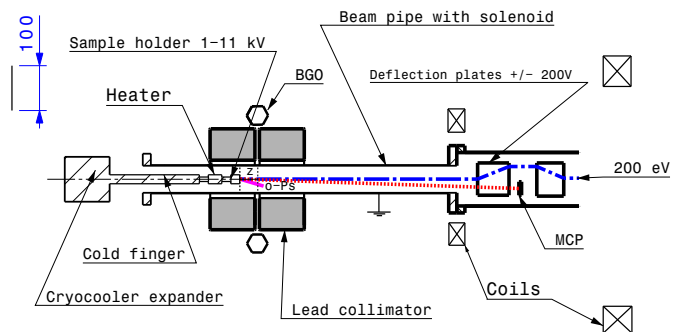


FIG. 1: *Experimental setup for the TOF measurements (the scale is in mm).*

The samples are mounted on a cryocooler head to allow the possibility of varying their temperature in the range of 50-400 K.

### B. PALS and TOF detectors

The start time  $t_0$  for the detectors is triggered by the MCP detecting the secondary electrons emitted when the positrons hit the target. In both PALS and TOF detectors the stop is given by one (or more) annihilation photons depositing some energy in the calorimeter (ECAL). Both ECAL are composed of BGO crystals with hexagonal shape, 61 mm external diameter and 200 mm length. The time resolution of the system MCP-ECAL was measured to be around 5 ns (FWHM). The typical energy resolution of the crystals is about 25-30% (FWHM). The

ECAL for the TOF is placed behind a lead slit at a distance  $z$  from the target that can be varied (as sketched in Figure 1). The detector is screened by four half cylinders of lead surrounding the beam pipe. The thickness of the shielding is 70 mm, the width of the slit is set to 5 mm and its position with respect to the target can be adjusted. For this measurement in order to maximize the signal to noise ratio the center of the slit was placed at a distance of 18 mm from the target. The determination of the slit position with respect to the target was done by scanning the slit position in 0.1 mm steps and recording the maximum of the 511 keV annihilation peak. The scans were performed 30 min after the temperature was set on the sample. This technique was very important in order to correct the slit position as a function of the temperature. In fact, at 50 K the contraction of the cryocooler head was measured to be  $1.30 \pm 0.05$  mm in agreement with the prediction of finite elements calculations performed with the COMSOL package [34]. The PALS detector was designed to have a large acceptance to provide a uniform efficiency for detecting the Ps emitted in vacuum [35].

### III. MONTE CARLO SIMULATIONS

In order to design the detectors and interpret the data, simulations served as a powerful tool. In the Monte Carlo (MC) simulations of our setup, the 3D EB-fields were calculated with the COMSOL multi-physics program and the positron/electron trajectories in the beam were simulated with GEANT4. The simulation of the photon detection in the apparatus was based on the same package [36]. New classes were written in order to simulate the o-Ps production, propagation in the beam pipe, reflection on pipe walls that were assumed to be Knudsen-like (Ps is reflected isotropically), pick-off effect or decay (Ps is not a standard particle in GEANT4). The events for the o-Ps  $\rightarrow 3\gamma$  process were generated taking into account the decay matrix element [37]. The geometries of the beam transport pipe, photon detector, positron tagging system and its material were coded into simulations. The results were cross-checked with our experimental measurements for both photon detection [4, 35, 38, 39] and particle transport in the EB-fields [33].

### IV. RESULTS

The measurements were taken in a clean vacuum of  $10^{-9}$  mbar. To avoid water contamination of the film during the cooling down, the target was kept at room temperature for an hour using a heater before lowering its temperature. The cooling cycles were repeated and the data confirmed the reproducibility of the results. The signals from the BGO's photomultipliers are split to record both energy and timing with a charge-to-digital converter (QDC CAEN v792) and a time-to-digital converter (TDC CAEN v775). A cut on the energy deposited

in the BGO between  $300 < E_{BGO} < 550$  keV was applied to optimize the signal to noise ratio suppressing the background coming from Compton scattering events in the collimator from annihilations in the target.

#### A. PALS measurements

In this section we present the results we obtained from the PALS measurements. The spectra are analyzed using the LT9 [41] program. The lifetimes of the decay components and its fractions are resolved by fitting the PALS spectra with 3 exponentials. The sum of the exponential functions is convoluted with a 5 ns FWHM resolution function of the spectrometer. We define as  $(\tau_2, I_2)$ , and  $(\tau_v, I_3)$  the intensities and the lifetimes of the two exponentials. To determine the yield  $Y_v$  of Ps emitted in vacuum and the lifetime  $\tau_f$  in the films we used a model of Ps escaping in vacuum [40]. According to this model the lifetime  $\tau_f$  in the films is defined as:

$$\tau_f = ((\tau_2^{-1} - \tau_v^{-1})I_2 / (I_2 + I_3) + \tau_v^{-1})^{-1} \quad (1)$$

The yield  $Y_v$  of Ps emitted in vacuum was calculated according to:

$$Y_v = (I_2 + I_3)\kappa_v / (\tau_f^{-1} + \kappa_v) \quad (2)$$

where

$$\kappa_v = (\tau_2^{-1} - \tau_v^{-1})I_3 / (I_2 + I_3) \quad (3)$$

is the escape rate of free Ps into vacuum. We extracted the films thicknesses for the two samples by fitting the total Ps yield as a function of the positron implantation energy to the Makhovian profile. These thicknesses are reported in Table I in which we also present the values of  $\tau_f$  and  $\kappa_v$  calculated with the expressions above. We use the results of the fits of the PALS spectra at 6 keV for the C sample and 10 keV for the F sample at 50 K and 300 K. These implantation energies will serve as a reference for the rest of the paper. We choose those values in order to maximize the amount of thermalized Ps. At these energies the majority of the positrons are still implanted within the films (see Fig. 2) and the emission energy is in the constant region (see next Section) With  $\tau_f$  one can calculate the effective pore size  $a$  in the films applying the Gidley et al. [7, 42] extension of the Tau-Eldrup model [43]-[46] (we will call it hereafter RTE model). As one can see, at lower temperature the lifetime in the film increases as predicted by the RTE model. This can be understood in the following way: the overlap of the Ps wave function with the volume contained within a distance  $\delta = 0.18$  nm [7, 42] from the walls for which the annihilation rate is assumed to increase is less for Ps confined in the pores occupying the ground state than for Ps in excited states. Since at lower temperatures the population of the ground state is higher the pick-off rate decreases. However, the measured lifetimes

are lower than what is expected by the calculations using the RTE model. For the C sample the discrepancy is less than 10% but for the F sample the measured value is 30% lower suggesting that the pick-off rate increases. Deviation from the RTE model were already observed in previous measurements using the 2 to 3 $\gamma$  ratio technique [47, 48] and in a measurement using PALS [49]. Different factors could be responsible for that as pointed out in those papers and deserves further studies.

Since the parameter  $\delta$  of the RTE model was calibrated at room temperature we use the lifetimes at 300 K to determine the effective pore size that Ps experiences in the pores. We report the results at the end of the paper in Table II for both rectangular channels and cubic boxes. Interestingly, we found that the yield of Ps emitted in vacuum can be considered as independent of the temperature of the target (see Fig. 2). This may seem to contra-

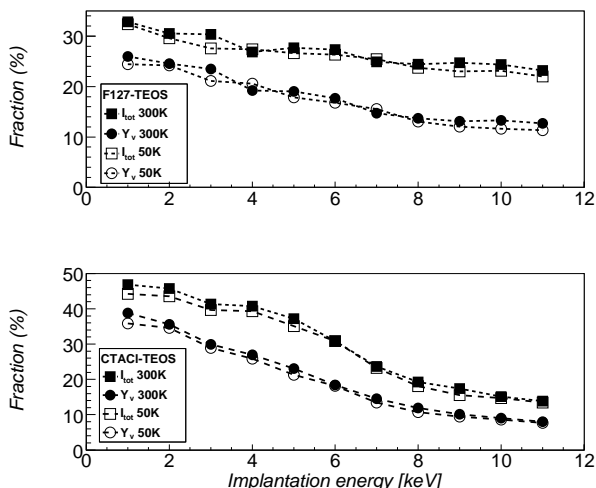


FIG. 2: Yield of Ps emitted in vacuum ( $Y_v$ ) and total yield of Ps ( $I_{tot} = I_2 + I_3$ ) for F (upper plot) and C sample (lower plot) at room temperature and 50K.

dict the fact that the lifetime in the films increases with the temperature. However, our measurements indicate that the escape rate in vacuum is smaller at lower temperature (see Table I), explaining the observation that the yield is constant. A possible explanation of this effect can be found considering that Ps tunnels from one pore to the other. In this case, the tunneling probability will decrease with temperature explaining our measurements.

## B. TOF measurements

Figure 3 shows the acquired TOF spectra at different implantation energies for the F sample. First we extract the mean energy of Ps emission in vacuum applying the analysis method proposed in [21] as follows.

TABLE I: Film thickness ( $Z$ ), Ps lifetime in the pores  $\tau_f$  and escape rate  $\kappa_v$  at 50 K and 300 K.

Sample	$Z$ [nm]	$\tau_f^{300K}$ [ns]	$\tau_f^{50K}$ [ns]	$\kappa_v^{300K}$ [ $\mu s^{-1}$ ]	$\kappa_v^{50K}$ [ $\mu s^{-1}$ ]
C	$700 \pm 200$	$54 \pm 1$	$60 \pm 1$	$27 \pm 1$	$25 \pm 1$
F	$1000 \pm 200$	$74 \pm 1$	$82 \pm 1$	$17 \pm 1$	$13 \pm 1$

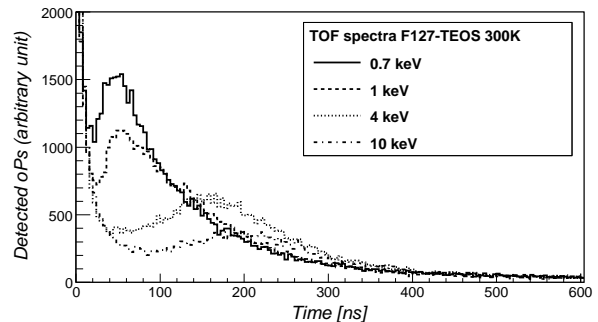


FIG. 3: TOF spectra of the F sample for positron implantation energies of 0.7-1-4-10 keV.

The background due to the annihilations in the target is subtracted by fitting the prompt peak with the resolution function of our detector determined using aluminum and kapton targets. The TOF spectra are corrected for the Ps decays and the time spent in front of the detector with the factor  $1/t \cdot e^{+t/\tau_{ops}}$ . The maximum of the peak distribution defines the mean Ps emission energy in the direction perpendicular to the film surface. Let us note that, neglecting the reflection of Ps in the beam pipe, with the time-of-flight method one measures only the mean of the energy component perpendicular to the collimator that we define as the z-axis (we define it as  $\langle E_z \rangle$ ). The triangles in Fig. 4, represent it as a function of the implantation energy. One can see that starting from 3 keV for the C sample (this was confirmed by other measurements on similar samples [51]) and 4 keV for the F sample the value of the energy emitted in vacuum tends to be constant. Clearly, the emission energy of Ps calculated in this way is not the minimal energy due to the confinement in the pores because one has different contributions given by the convolution of the emission energy with the implantation profile. In order to isolate the thermalized part from the TOF spectra, one has to subtract the contributions of non-thermalized Ps components (see Fig. 5). To estimate these non-thermalized contributions, we suppose that the shape of their distribution, NT(t), is represented by the TOF spectrum obtained at a low implantation energy. We choose 2 keV in the case of the C sample, and 3 keV for the F sample. At these energies 95% of the positrons are implanted at depths smaller than  $L_{2keV} = 200$  nm and  $L_{3keV} = 350$  nm, as calculated from a Makhovian profile taking into account the

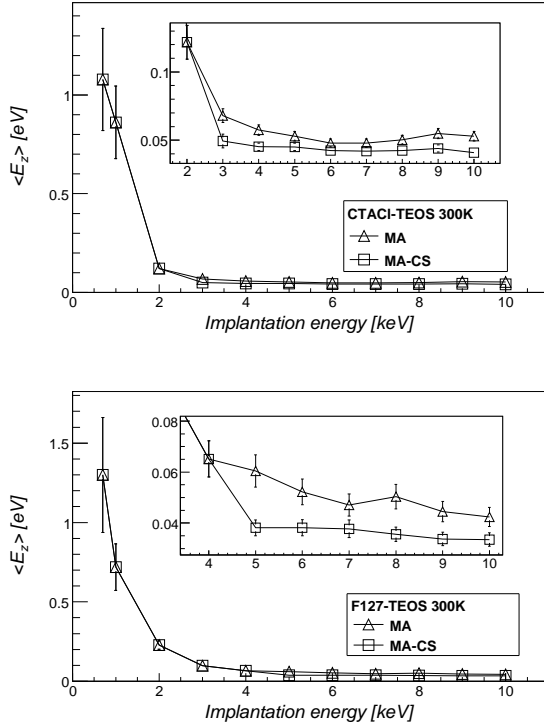


FIG. 4: Positronium mean emission energy  $\langle E_z \rangle$  as a function of the implantation voltage at a target temperature of 300K. The triangles represents the energy extracted with the maximum analysis method (MA), the squares are after the subtraction of the non-thermalized part (maximum analysis method after correction of the spectra, MA-CS).

film thickness. For a given implantation energy  $E_i$ ,  $NT(t)$  is scaled down by the fraction of positrons implanted at depths smaller than  $L_{2keV}$  and  $L_{3keV}$ .

The results of this analysis are shown as the squares in Fig. 4. A parabolic fit is used to determine the position of the maximum. The statistical error of the fit is typically  $\pm 9$  ns for the F and  $\pm 6$  ns for the C sample. The uncertainty on the determination of the slit position of  $\pm 0.1$  mm results in a systematic error of the order of  $\pm 1$  meV in the determination of the Ps mean emission energy  $\langle E_z \rangle$  (for implantation energies above 3 keV). Thus the combined statistical and systematic error is at a level of  $\pm 2.5$  meV for the F and  $\pm 1.9$  meV for the C sample.

The results for the C and the F samples at room temperature and at 50 K are shown in Figs. 6-7. For implantation energies higher than 4 keV for the C and 5 keV for the F sample the values  $\langle E_z \rangle$  of the mean emission energy are constant. In the C sample,  $\langle E_z \rangle$  reaches its constant value at lower implantation voltages because the pore size is smaller than in the F sample (see Fig. 6). Those values are higher than the thermal energy that Ps will have if it would thermalize at the temperature of

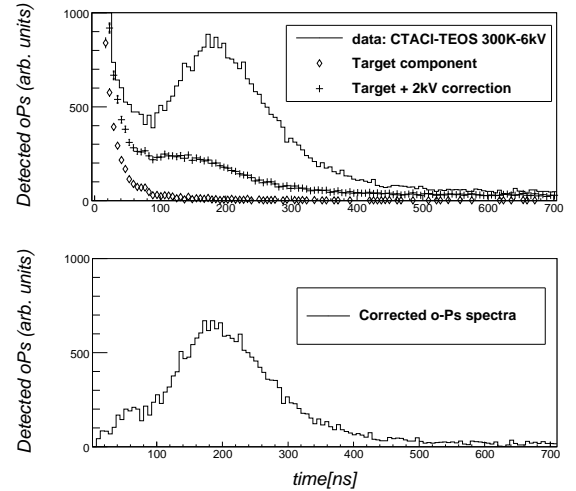


FIG. 5: Upper plot: the solid line is the TOF spectra without correction, the diamonds is the contribution from the target and the crosses is the sum of the contribution from the target and the non-thermalized part. Lower plot: the TOF spectra after the correction of the target and the non-thermalized components.

the film. As expected in the presence of confinement in the pores, the mean emission energy is higher for the C sample with pore sizes smaller than the F sample. To understand the behavior of the value of the minimal energy as a function of the film temperature we present a simple model of Ps in thermodynamic equilibrium at a temperature  $T$  in rectangular boxes.

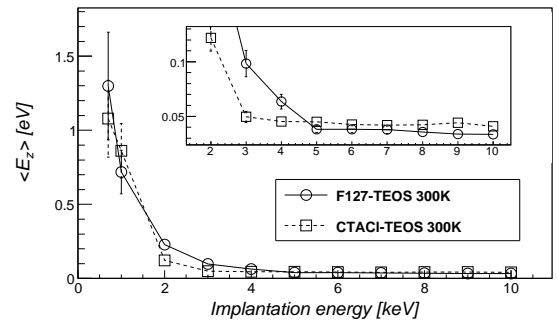


FIG. 6: Ps mean emission energy  $\langle E_z \rangle$  as a function of the positron implantation voltage for C and F sample at 300 K.

The expectation value  $\langle H \rangle$  of the Hamiltonian operator for Ps confined in 1 dimensional infinite well in contact with a reservoir at a temperature  $T$  is given by:

$$\langle H \rangle = kT^2 \frac{1}{Z} \frac{dZ}{dT} \quad (4)$$

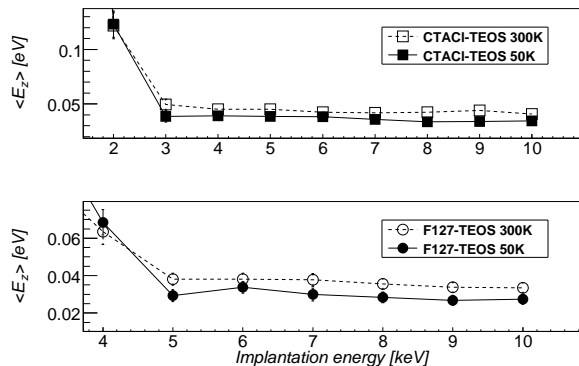


FIG. 7: Upper plot: Ps mean energy  $\langle E_z \rangle$  for implantation energies higher than 2 keV at 50 K and 300 K for the C sample. Lower plot: Ps mean energy as a function of the implantation energies higher than 4 keV at 50 K and 300 K for the F sample.

where  $Z$  is the partition function defined as

$$Z(a) = \sum_{n=1}^{\infty} e^{-\frac{h^2 n^2}{8ma^2}/kT} \quad (5)$$

where  $a$  is the dimension of the well,  $m$  is the Ps mass and  $h$  and  $k$  are the Plank and the Boltzmann constants. To calculate the mean value  $\langle H \rangle$  of the energy for the 3D case we can use

$$\langle H \rangle = \langle H_x \rangle + \langle H_y \rangle + \langle H_z \rangle \quad (6)$$

where to calculate  $\langle H_y \rangle$  and  $\langle H_z \rangle$  one can substitute the pore side length  $a$  in Eq.5 with  $b$  and  $c$ . For Ps confined in rectangular pores, we thus obtain:

$$\langle H \rangle = kT^2 \left( \frac{1}{Z(a)} \frac{dZ(a)}{dT} + \frac{1}{Z(b)} \frac{dZ(b)}{dT} + \frac{1}{Z(c)} \frac{dZ(c)}{dT} \right) \quad (7)$$

For the case of a cubic box one can set  $\langle H_x \rangle = \langle H_y \rangle = \langle H_z \rangle$ . When Ps is emitted in vacuum the confinement energy converts in kinetic energy. The results of the TOF is the mean energy detected in the  $z$ -direction. To compare the experimental data with the model described above one has to multiply by a factor  $\xi$  that takes into account the angular distribution of the emitted Ps and the reflection of Ps in the beam pipe. Furthermore, the simulation takes into account the detector acceptance. This is important because the probability that events decaying before or after the collimator aperture are detected is not negligible. To determine  $\xi$  we used our MC simulation assuming that Ps is emitted mono-energetically and isotropically from the surface of the films. The validity of the simulation is cross-checked comparing the data with the spectra simulated using the yield of Ps in vacuum measured with the PALS technique. As shown in the upper plot of Fig. 8 a satisfactory agreement is achieved. We attribute the difference between 40

and 100 ns to the approximation done in the subtraction method where the contribution of the non-thermalized is underestimated since only a spectrum of a defined energy is used for this correction. The fact that the Ps is emitted with an angular spread is clearly supported by the data. As one can see in the lower plot of Fig. 8 for Ps emitted with no angular spread the data are not reproduced. The physical interpretation is that in the films we studied the pores have no organization thus they are expected to be randomly aligned. The value of  $\xi$  estimated with the MC is about 1.7.

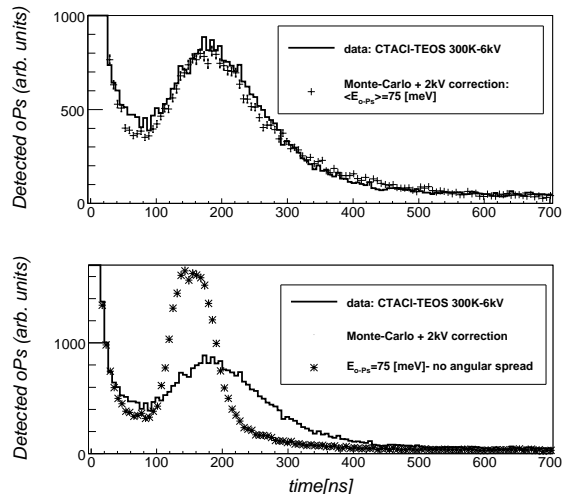


FIG. 8: Upper plot: comparison between the data of the C sample at 6 keV and the MC simulating mono-energetic Ps emitted isotropically from the film surface. Lower plot: comparison between the data of the C sample at 6 keV and the MC simulating mono-energetic Ps emitted perpendicular from the film surface. In both cases, the measured non thermalized part was added to the MC.

A detailed scan shows that the mean Ps energy ( $\langle E_{PS} \rangle = \xi \langle E_z \rangle$ ) decreases with the sample temperature down to a minimum level (see Fig. 9). For the C sample this value is basically constant ( $73 \pm 4$  meV) in the range of temperature in which we performed our measurement. This can be understood by the fact that in this sample the confinement energy is much higher than the thermal energy at room temperature ( $kT \simeq 25$  meV) thus almost all Ps is in the ground state. For the F sample there is a weak dependence on the temperature. Due to the bigger pore size compared to the C sample, the energy of the ground state is only twice the thermal energy at room temperature. Therefore, the probability to find the Ps occupying an excited state is higher. As expected, this probability decreases with the temperature thus the minimal energy reaches its constant value of  $48 \pm 3$  meV.

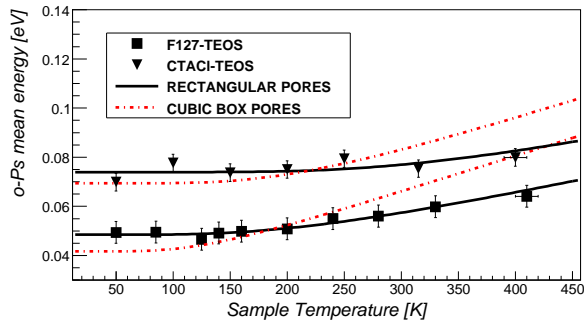


FIG. 9: Positronium mean energy as a function of the mesoporous film temperature. Those results are obtained at 6 keV for the C and 10 keV for the F sample. The solid lines are the results of the using Eq. 7 with the pore side lengths  $a, b, c$  left as free parameters. The dashed lines were obtained fitting with Eq. 7 with a single side length free  $a = b = c$  (cubic box pores).

### C. Discussion

To compare the prediction of the pore size that one can extract from the TOF measurements with the PALS results we fit the data using Eq. 7. The solid lines in Fig. 9 represent the fit to the data where the pore side length ( $a, b, c$ ) are left as free parameters. The fits were repeated assuming cubic box pores and the results are shown as the dashed lines in Fig. 9. We used MIGRAD from the MINUIT package [50] as a minimization procedure. As one can see, the fit to the data suggests that the pores of both samples are better modeled as rectangular pores than cubic boxes. As proposed in [51], to compare the values obtained from the fit with the ones extracted from the PALS measurements, one has to add twice the parameter  $\delta$  (see previous Section). The pores side lengths obtained in this way are reported in Table II. In particular, the fit supports the idea that the pores are better modeled by rectangular channels. The pore side length in one direction ( $c$ ) obtained from the fit is much longer than the substrate thickness. Since, the same values for the side length  $a$  and  $b$  are obtained fitting the data assuming rectangular channels instead of rectangular boxes we do not report this value in Table II that has no physical meaning.

According to the quantum mechanical model for Ps thermalization of Mariuzzi et al. [18] the index  $n$  in the sum of Eq. 5 could differ from 1 for cubic pores if the level separation of two close Ps energy levels is higher than the maximum momentum that a single phonon can exchange. We performed fits with different  $n > 1$  but the results did not improve, supporting the idea that the pores are not very well modeled by cubic boxes. To summarize, for the C sample with the TOF data the best fit was obtained for pores modeled as square channels of

TABLE II: Comparison of the pore sizes obtained from the PALS measurements at 300 K and from the fit of the Ps mean emission as a function of the temperature of the sample (see Fig. 9) for both cubic box (BOX) and rectangular pores (RECT). Minimal energy of Ps  $\langle E_{Ps} \rangle$  for which the errors are the combined statistical and systematic error.

C Sample		
	TOF	PALS
$a_{BOX}$ [nm]	$3.3 \pm 0.1$	$4.2 \pm 0.5$
$(a, b)_{RECT}$ [nm]	$(2.7 \pm 0.5, 2.7 \pm 0.5)$	$(3.3 \pm 0.5, 3.3 \pm 0.5)$
$\langle E_{Ps} \rangle$ [meV]	$73 \pm 4$	
F Sample		
	TOF	PALS
$a_{BOX}$ [nm]	$4.1 \pm 0.1$	$6.4 \pm 0.5$
$(a, b)_{RECT}$ [nm]	$(2.9 \pm 0.6, 3.6 \pm 1.5)$	$(4.3 \pm 0.5, 5.3 \pm 0.5)$
$\langle E_{Ps} \rangle$ [meV]	$48 \pm 3$	

$2.7 \pm 0.5$  nm side length while the lifetime method gives  $3.3 \pm 0.5$  nm. The best fit to the data for the F sample was obtained for rectangular channels with a cross section of  $2.9 \pm 0.6$  nm by  $3.6 \pm 0.6$  nm that has to be compared with  $4.3 \pm 0.5$  by  $5.3 \pm 0.5$  of the PALS measurement. This pore size was extracted by applying the RTE model to reproduce the measured lifetime of 74 ns assuming the ratio  $a/b$  to be the same as in the TOF results. Both values obtained with the TOF measurement are systematically lower than the PALS results. Nevertheless, considering the approximation done in our model, the assumptions that the pores can be treated as rectangular channels and the uncertainty in the determination of the pore size we conclude that our results (summarized in Table II) are in a reasonable agreement with the expectations.

### V. CONCLUSIONS

In this paper, we show that the yield of Ps emitted in vacuum measured with the PALS technique is independent of the temperature of the mesoporous thin films. The lifetime in the films increases with a decrease in temperature but the measured values are lower than expected by the RTE model. This suggests that another source of pick-off which depends on the temperature should be invoked. Further studies are needed to investigate the origin of this effect. The escape rate in vacuum decreases explaining the observation that the yield of Ps emitted in vacuum is the same at 50 and 300 K.

Furthermore, we show that due to quantum mechanical confinement in the pores the Ps emission energy into vacuum has a minimal value. The minimal energy is higher for the sample with smaller pores and this constant value is reached at a lower positron implantation energy. Our results are in fair agreement with a model of Ps confined in rectangular channels in thermal equilibrium with the sample. The measured minimal energy for the C sample was found to be  $73 \pm 4$  meV while for the F sample it is  $48 \pm 3$  meV. These experimental results

provide a solid ground to understand how to produce Ps at lower temperature and could serve to develop a more realistic model to interpret the data.

### Acknowledgments

This work was supported by the Swiss National Foundation and ETH Zurich and the CNPq (Brazil). P.C.

would like to thank C. Lenz Cesar, P. Lotti and B. Barbiellini for the very useful discussions.

- 
- [1] M. Deutsch, *Phys. Rev.* **82**, 455 (1951).
- [2] S. Karshenboim, *Int. J. Mod. Phys. A* **19**, 3879 (2004).
- [3] A. Rubbia, *Int. J. Mod. Phys. A* **19**, 3961 (2004) [arXiv:hep-ph/0402151].
- [4] A. Badertscher, P. Crivelli, W. Fetscher, U. Gendotti, S. Gninenko, V. Postoev, A. Rubbia, V. Samoylenko, D. Sillou, *Phys. Rev. D* **75**, 032004 (2007) [arXiv:hep-ex/0609059].
- [5] S.W.H. Eijt, B. Barbiellini, A.J. Houtepen, D. Vanmaekelbergh, P.E. Mijnaerends, A. Bansil, *Phys. Stat. Sol. (c)* **4**, 3883 (2007), arXiv:0705.1113v1.
- [6] D. W. Gidley, H. G. Peng, R. S. Vallery *Annual Review of Materials Research* **36**, 49 (2006).
- [7] D. W. Gidley, W. E. Frieze, T. L. Dull, A. F. Yee, E. T. Ryan, and H. M. Ho, *Phys. Rev. B* **60**, R5157 (1999).
- [8] D. W. Gidley, W. E. Frieze, T. L. Dull, J. Sun, A. F. Yee, C. V. Nguyen, and D. Y. Yoon, *Appl. Phys. Lett.* **76**, 1282 (2000).
- [9] D. B. Cassidy, H. W. K. Tom and A. P. Mills, *AIP Conf. Proc.* **1037**, 66 (2008).
- [10] A. Kellerbauer et al. [AEGIS Collaboration], *Nucl. Instr. and Meth. B* **266**, 351 (2008).
- [11] P. Perez, L. Liskay, M. F. Barthe, J.-P. Boilot, M. Carty, C. Corbel, P. Crivelli, A. Curtioni, O. Delferriere, P. Desgardin, M. Etienne, U. Gendotti, M. Hassan, A. Mohri, T. Ohdaira, J.-M. Rey, A. Rubbia, H. Saitoh, Y. Sauce, R. Suzuki, A. Walcarius, and Y. Yamazaki, *AIP Conf. Proc.* **1037**, 35 (2008).
- [12] R. Bernabei et al. [DAMA Collaboration], *Eur. Phys. J. C* **56**, 333 (2008). [arXiv:0804.2741 [astro-ph]].
- [13] R. Foot, *Phys. Rev. D* **78**, 043529 (2008) [arXiv:0804.4518 [hep-ph]].
- [14] A. Badertscher, A. Belov, P. Crivelli, S. N. Gninenko, J. P. Peigneux, A. Rubbia and D. Sillou, *Int. J. Mod. Phys. A* **19** 3833 (2004).
- [15] A. P. Mills, Jr., L. Pfeier, and P. M. Platzman, *Phys. Rev. Lett.* **51**, 1085 (1983).
- [16] S. Valkealahti and R. Nieminen, *Appl. Phys. A* **32** (1983), p. 95.
- [17] Y. Nagashima, Y. Morinaka, T. Kurihara, Y. Nagai, T. Hyodo, T. Shidara, and K. Nakahara, *Phys. Rev. B* **58**, 12676 1998.
- [18] S. Mariuzzi, A. Salemi and R. S. Brusa, *Phys. Rev. B* **78**, 085428 (2008).
- [19] M. Tuomisaari, R. H. Howell, and T. McMullen, *Phys. Rev. B* **40**, 2060 (1989).
- [20] Y. Nagashima et al., *Phys. Rev. B* **58**, 12676 (1998).
- [21] A. P. Mills, Jr., E. D. Shaw, R. J. Chichester, and D. M. Zuckerman, *Phys. Rev. B* **40**, 2045 (1989).
- [22] R. S. Yu, T. Ohdaira, R. Suzuki, K. Ito, K. Hirata, K. Sato, Y. Kobayashi, and J. Xu, *Appl. Phys. Lett.* **83**, 4966 (2003).
- [23] K. Ito, R. S. Yu, K. Sato, K. Hirata, Y. Kobayashi, T. Kurihara, M. Egami, H. Arao, A. Nakashima, and M. Komatsu, *J. Appl. Phys.* **98**, 094307 (2005).
- [24] C. He, M. Muramatsu, N. Oshima, T. Ohdaira, A. Kinomura, and R. Suzuki, *Phys. Lett. A* **355**, 73 (2006).
- [25] M. P. Petkov, M. H. Weber, K. G. Lynn, and K. P. Rodbell, *Appl. Phys. Lett.* **79**, 3884 (2001).
- [26] R. Suzuki, T. Ohdaira, Y. Kobayashi, K. Ito, R. S. Yu, Y. Shioya, H. Ichikawa, H. Hosomi, K. Ishikiriyama, H. Shirataki, S. Matsuno, and J. Xu, *Mater. Sci. Forum* **445-446**, 224 (2004).
- [27] J. Xu, A. P. Mills, Jr., and C. Case, *Appl. Phys. Lett.* **87**, 54105 (2005).
- [28] H. K. M. Tanaka, T. Kurihara, and A. P. Mills, Jr., *Phys. Rev. B* **72**, 193408 (2005).
- [29] C. He, T. Ohdaira, M. Muramatsu, N. Oshima, A. Kinomura, R. Suzuki, T. Oka and Y. Kobayashi *Phys. Rev. B* **75**, 195404 (2007).
- [30] L. Liskay, C. Corbel, P. Perez, P. Desgardin, M.-F. Barthe, T. Ohdaira, R. Suzuki, P. Crivelli, U. Gendotti, A. Rubbia, M. Etienne, and A. Walcarius, *Appl. Phys. Lett.*, **92**, 063114 (2008).
- [31] Y. Cohen, K. Landskron, N. Tetreault, S. Fournier-Bidoz, B. Hatton, G. A. Ozin, *Adv. Funct. Mater.* **15**, 593 (2005).
- [32] W. Yantasee, Y. Lin, X. Li, G. E. Fryxell, T. S. Zemanian and V. V. Viswanathan, *Analyst*, **128**, 899 (2003).
- [33] N. Alberola, T. Anthonioz, A. Badertscher, C. Bas, A.S. Belov, P. Crivelli, S.N. Gninenko, N.A. Golubev, M.M. Kirsanov, A. Rubbia and D. Sillou, *Nucl. Instr. Method A* **560**, 224 (2006).
- [34] <http://www.comsol.com/>
- [35] P. Crivelli, U. Gendotti, L. Liskay, P. Perez, A. Rubbia, *Mat. Sci. Forum*, Vol. 607 pg. 251 (2009).
- [36] GEANT4 collaboration, *Nucl. Instr. Method A* **506**, (2003), 250-303
- [37] A. Ore and J. L. Powell, *Phys. Rev.* **75**, 1696 (1949).
- [38] A. Badertscher, P. Crivelli, M. Felcini, S.N. Gninenko, N.A. Goloubev, P. Nedelec, J.P. Peigneux, V.Postoev, A. Rubbia and D. Sillou *Phys. Lett. B* **542**, 29 (2002).
- [39] P. Crivelli, "A new search for invisible decays of orthopositronium", PhD Thesis, No.16617, ETH Zurich, Switzerland (2006).
- [40] L. Liskay, C. Corbel, L. Raboin, J.-P. Boilot, P. Perez, A. Brunet-Bruneau, P. Crivelli, U. Gendotti, A. Rubbia, T. Ohdaira and R. Suzuki, *Appl. Phys. Lett.* **95**, 124103 (2009).
- [41] Kansy, J., *Nucl. Instrum. Meth. A* **374**, 235 (1996).



- [42] L. Dull, W. E. Frieze, D. W. Gidley, J. Sun, and A. F. Yee, *J. Phys. Chem. B* 105, 4657 (2001).
- [43] S. J. Tau, *Chem. Phys. Lett.* 56, 5499, (1972).
- [44] M. Eldrup, D. Lighbody and J. N. Sherwood, *Chem. Phys. Lett.* 63, 51, (1981).
- [45] T. Goworek, K. Ciesielski, B. Jasinska, and J. Wawryszczuk, *Chem. Phys. Lett.* 272, 91 (1997).
- [46] K. Ito, H. Nakanishi and Y. Ujihira *J. Phys. Chem. B* 103, 4555-4558 (1999).
- [47] S. Mariazzi, L. Toniutti, N. Patel, R.S. Brusa, *Applied Surface Science* 255 (2008) 191193.
- [48] C. G. Fischer, M. H. Weber, C. L. Wang, S. P. McNeil, and K. G. Lynn, *Phys. Rev. B* 71, 180102R 2005.
- [49] S. Thraenert, E. M. Hassan, D. Enke, D. Fuerst and R. Krause-Rehberg, *Phys. Status Solidi C* 4, 3819 (2007).
- [50] F. James, M. Roos, MINUIT, *Function Minimization and Error Analysis*, CERN D506 (Long Writeup).
- [51] D. B. Cassidy, P. Crivelli, T. H. Hisakado, L. Liskay, V. E. Meligne, P. Perez, H. W. K. Tom, and A. P. Mills Jr., *Phys. Rev. A* 81, 012715 (2010).